# Supporting Information

## Engineering Dimensionality and Band-Edges with Lone-Pair Cations to Achieve Superior X-ray Detection in Metal-Free Perovskites

Jiasheng Gong,[a,b] Chensheng Lin,[a] Chunlei Yu,[a] Pengxiang Dong,[c] Tao Yan,[a] Huixin Fan*[a] and Min Luo*[a]

[a] State Key Laboratory of Functional Crystals and Devices, Fujian Institute of Research on the Structure of Matter, Chinese Academy of Sciences, Fuzhou, Fujian 350002, China.

[b] Fujian College, University of Chinese Academy of Sciences, Fuzhou, Fujian 350002, China

[c] School of Materials Science and Engineering, Nankai University, Tianjin 300350, China

E-mail: lm8901@fjirsm.ac.cn (Min Luo), huixinfan@fjirsm.ac.cn (Huixin Fan)

**Experimental:**

**Materials preparation:** Ammonium tetrafluoroborate ($NH_4BF_4$, 99%), hydrazine monohydrochloride ($N_2H_5Cl$, 98%), tetrafluoroboric acid ($HBF_4$, 40%), and N-N′-diazabicyclo[2.2.2] octane (DABCO, 98%) were purchased from Adamas Reagent. All reagents and chemicals were used as received without further purification.

**Synthesis of DABCO-$NH_4(BF_4)_3$ powders:** DABCO (1.12 g, 10 mmol), $NH_4BF_4$ (1.05 g, 10 mmol), and $HBF_4$ (40%, 5 mL) were dissolved in 25 mL $H_2O$ and stirred at room temperature for 24 h. The mixed solution was evaporated using a rotary evaporator at 60°C, then the white precipitate was collected, washed with methanol several times. Finally, the white product was dried for 24 hours at 50°C in a vacuum oven.

**Synthesis of DABCO-$N_2H_5(BF_4)_3$ powders:** The synthesis was performed following the same procedure as for DABCO-$NH_4(BF_4)_3$, with the only replacement of $NH_4BF_4$ with $N_2H_5Cl$ (0.68 g, 10 mmol). Additionally, the reaction was conducted in 10 mL $H_2O$ and stirred for 12 h, with subsequent evaporation, washing, and drying steps remaining identical.

**Synthesis of DABCO-$NH_4(BF_4)_3$ SCs:** The DABCO-$NH_4(BF_4)_3$ single crystals were grown by dissolving the DABCO-$NH_4(BF_4)_3$ powders into deionized water to form a saturated solution. Then, the impurities in the mixture solution were removed by filtration, and the clear filtrate was transferred into a crystallizing dish and held at a constant temperature of 40℃ in the oven for several days to afford single crystals.

**Synthesis of DABCO-$N_2H_5(BF_4)_3$ SCs：** The DABCO-$N_2H_5(BF_4)_3$ single crystals were grown by dissolving the DABCO-$N_2H_5(BF_4)_3$ powders into deionized water to form a saturated solution. Then, the impurities in the mixture solution were removed by filtration, and the clear filtrate was transferred into a crystallizing dish and held at a constant temperature of 35℃ in the oven for several days to afford single crystals.

**Single-Crystal Structure Determination:** Single crystal of DABCO-$NH_4(BF_4)_3$ and DABCO-$N_2H_5(BF_4)_3$ were selected for single-crystal X-ray diffraction (SCXRD) measurements, with diffraction data collected on a Rigaku Mercury CCD diffractometer at room temperature. The diffractometer was equipped with graphite-monochromatized Cu Kα radiation (λ = 1.54184 Å). Data reduction was implemented via the CrysAlisPro software package, and absorption corrections were applied using the multi-scan method. The crystal structure was solved by direct methods and refined through full-matrix least-squares fitting on $F^2$ with SHELXL within the OLEX2[1] program suite. Structural validation was performed using the PLATON[2] software. Crystallographic data and structure refinement details for DABCO-$NH_4(BF_4)_3$ and DABCO-$N_2H_5(BF_4)_3$ were summarized in Table S3, while atomic coordinates, equivalent isotropic displacement parameters, selected bond lengths and angles, as well as anisotropic displacement parameters are provided in Tables S4-S9.

**Powder X-ray diffraction (PXRD):** X-ray diffraction (XRD) patterns of the polycrystalline samples were collected on a Miniflex600 powder diffractometer with Cu Kα radiation (λ = 1.540598 Å) at room

temperature, covering a $2\theta$ range of 10-60° with a scanning step size of 0.02°. The experimental and simulated powder XRD patterns of DABCO-$NH_4(BF_4)_3$ and DABCO-$N_2H_5(BF_4)_3$ were presented in Figures S2-S3.

**Energy-dispersive X-ray Spectroscopy Analysis**: Microprobe elemental analyses were performed by a field emission scanning electron microscope (FESEM, SU-8010) with energy dispersive X-ray spectroscope. The DABCO-$NH_4(BF_4)_3$ and DABCO-$N_2H_5(BF_4)_3$ crystals were washed by alcohol and mounted on an aluminum sample stage (Figures S6-S7).

**Thermal analysis:** Thermogravimetric Analysis (TGA) was performed by using a Netzsch STA449F3 simultaneous analyzer under flowing $N_2$ at a rate of 10°C·min$^{-1}$. The DABCO-$NH_4(BF_4)_3$ and DABCO-$N_2H_5(BF_4)_3$ polycrystalline samples were placed in an $Al_2O_3$ crucible with another empty $Al_2O_3$ crucible used as the reference, and heated from 30°C to 550°C (Figures S8-S9).

**First-principles calculations:**

Band structure and partial density of states (PDOS) calculations for DABCO-$NH_4(BF_4)_3$ and DABCO-$N_2H_5(BF_4)_3$ were performed via the CASTEP[3] code, a plane-wave pseudopotential total energy package based on density functional theory (DFT).[4] The regularized Strongly Constrained and Approximately Correct (rSCAN) functional within the meta-generalized gradient approximation (m-GGA) was adopted to describe the exchange-correlation energy. A high plane-wave kinetic energy cutoff of 898.0 eV and a Monkhorst-Pack[5] k-point mesh of 2 × 2 × 1 were carefully selected for numerical integration over the Brillouin zone. Calculations of electron density, charge distribution and electrostatic interactions were conducted using the CP2K package,[6] while the climbing image nudged elastic band (CI-NEB) method was employed to determine the potential barrier energy.[7] Defect formation energy was calculated according to formula (1),[8] and the independent gradient model based on Hirshfeld partition (IGHM)[9] diagrams were plotted using the Multiwfn[10] and VMD[11] software packages.

$$E = E_{defect} - E_0 - \sum_i n_i\mu_i + q(E_f - E_{VBM}) \quad (1)$$

The $E_{defect}$ and $E_0$ represent the total energies of the same supercell with and without defects, respectively. The $n_i$ represents the change in the number of atoms introduced as a defect. The $\mu_i$ represents chemical potential of element i. The $E_f$ and $E_{VBM}$ represent the Fermi level and the energy of the valence band top of a perfect crystal, respectively.

**Device parameters:**

**μτ product calculation:** In this work, a device structure of Ag/DABCO-$NH_4(BF_4)_3$ SC/Ag and Ag/DABCO-$N_2H_5(BF_4)_3$ SC/Ag were used for photoconductivity measurement. Then, the simplified Hecht equation (2) was utilized to extract the μτ product from photoconductivity curves, as follows:

$$I = \frac{I_0\mu\tau V}{d^2}[1 - exp(-\frac{d^2}{\mu\tau V})] \quad (2)$$

where $I_0$ is the saturated photoinduced current, V is the bias voltage, and d is the device thickness.

**X-ray detectors**: X-ray detection measurements were conducted on a modified Super Nova setup, with X-rays emitted from a tungsten anode tube operating at a fixed accelerating voltage of 40 keV. All X-

ray response characterizations were performed in a dark environment shielded by a blackout curtain, and the photocurrent was recorded via a high-precision Keithley 6517B electrometer. All tests were carried out at room temperature.

**Signal-to-noise ratio (SNR) calculation:** The SNR is calculated according to the relation: SNR = $I_{signal}/I_{noise}$, where the signal current ($I_{signal}$) is the difference between the average photocurrent and the average dark current, and the noise current ($I_{noise}$) is obtained by calculating the standard deviation of the photocurrent.

**Dark current drift (*D*) calculation:** The *D* is calculated according to the relation $D=|J_{finish}-J_{begin}|/(t\times E)$, where *t* is duration, *E* is applied electric field, $J_{finish}$ and $J_{begin}$ represent current density at the end and beginning, respectively.

**Gain factor calculation:** The gain factor can be calculated as follows:

$$\text{Gain factor} = \frac{I_R}{I_P}$$

where $I_R$ and $I_P$ stand for induced photocurrent and theoretical photocurrent under X-ray illumination. $I_R$ can be obtained in the experiment, while $I_P$ should calculate as formula (3):

$$I_P = \varphi\beta e \tag{3}$$

The $\varphi$ (photon absorption rate) is defined as: $$\varphi = \frac{\varepsilon D m_s}{E_{ph}}$$

where $\beta$ (the number of excited carriers per X-ray photon) is defined as: $$\beta = \frac{E_{ph}}{1.43 + 2E_g}$$

Notably, *e* represents electric charge, ε is the photon absorption fraction of the sample, *D* represents the dose rate, $m_s$ is the mass of the sample, and $E_{Ph}$ is X-ray energy, $E_g$ represents the band gap.

Goldschmidt tolerance factor calculation:

$$t = \frac{R_A + R_X}{\sqrt{2}(R_B + R_X)} \tag{4}$$

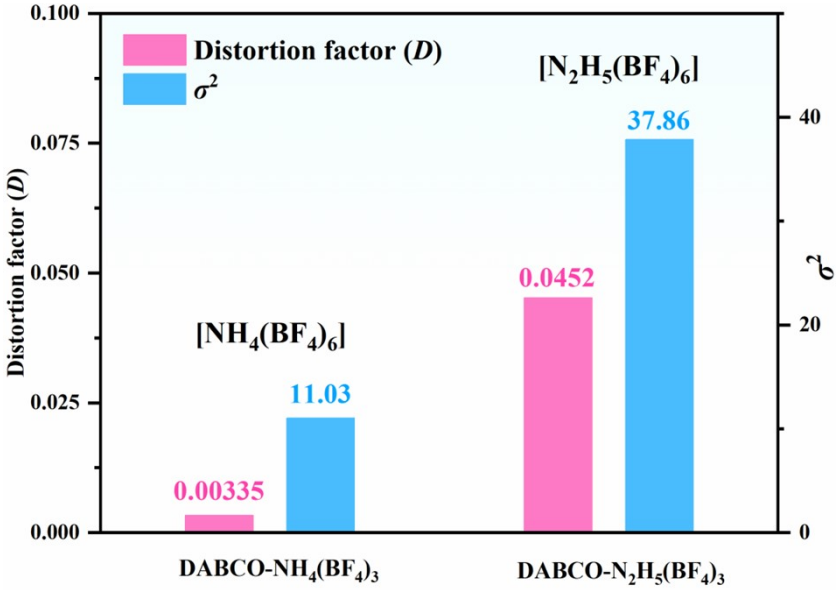


**Figure S1.** The comparison of distortion factors and bond angle variances of adjacent octahedra in DABCO-$NH_4(BF_4)_3$ and DABCO-$N_2H_5(BF_4)_3$.

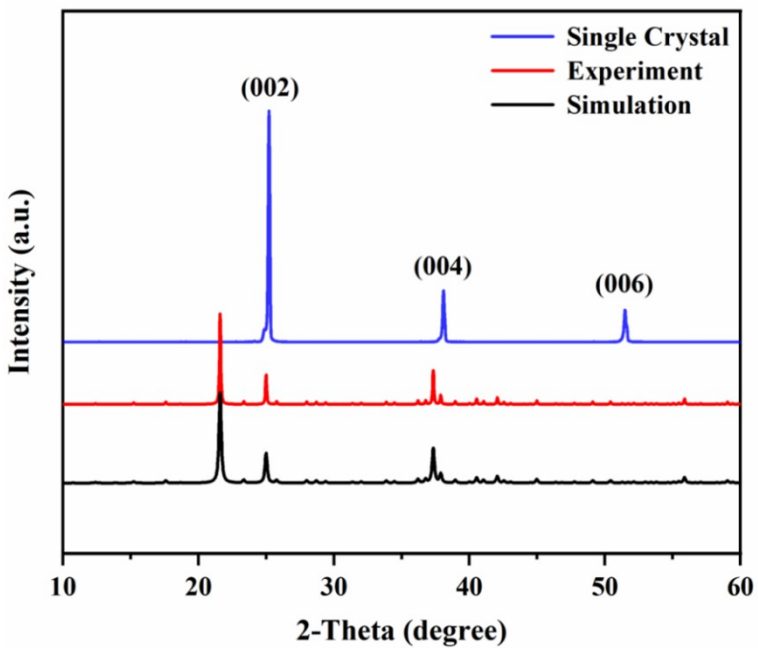


**Figure S2.** X-ray diffraction patterns of DABCO-$NH_4(BF_4)_3$ single crystal and its simulated and experimental powder.

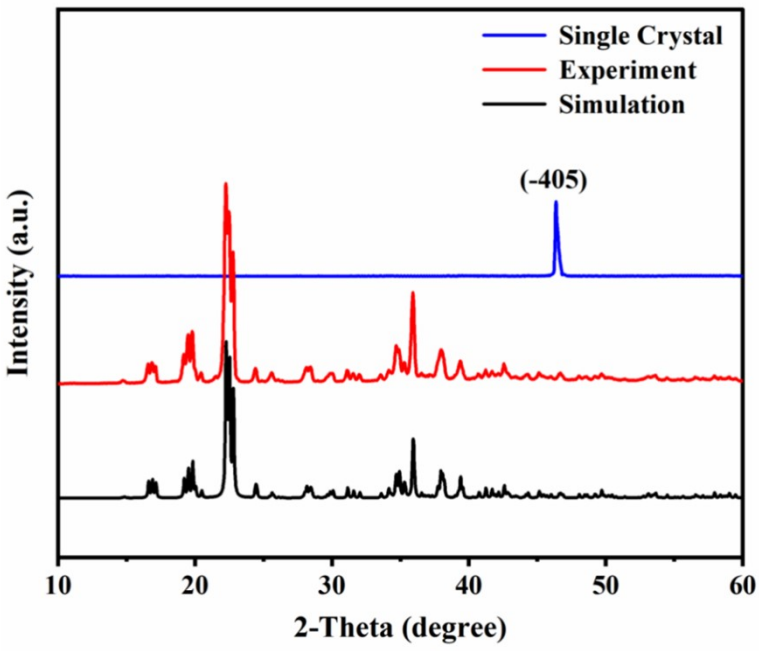


**Figure S3.** X-ray diffraction patterns of DABCO-$N_2H_5(BF_4)_3$ single crystal and its simulated and experimental powder.

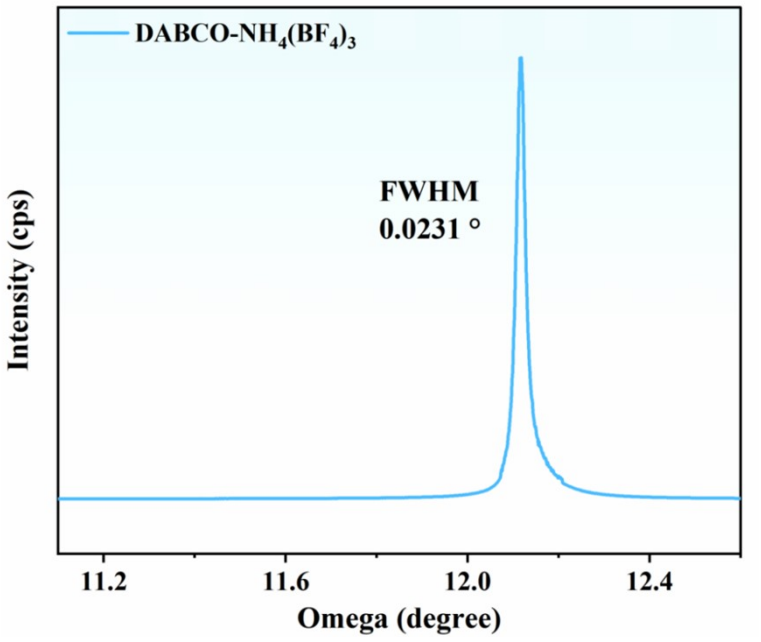


**Figure S4.** High-resolution XRD rocking curve of DABCO-$NH_4(BF_4)_3$ on (002) plane.

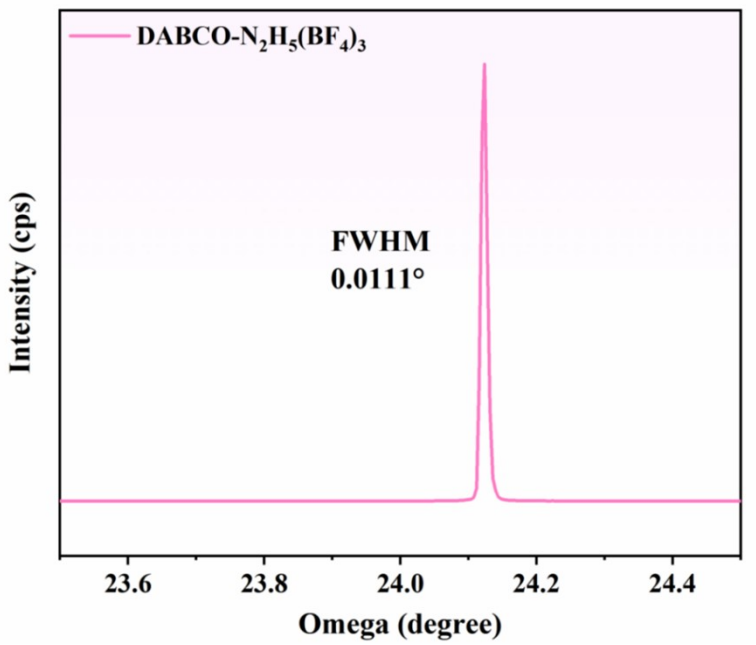


**Figure S5.** High-resolution XRD rocking curve of DABCO-$N_2H_5(BF_4)_3$ on (-405) plane.

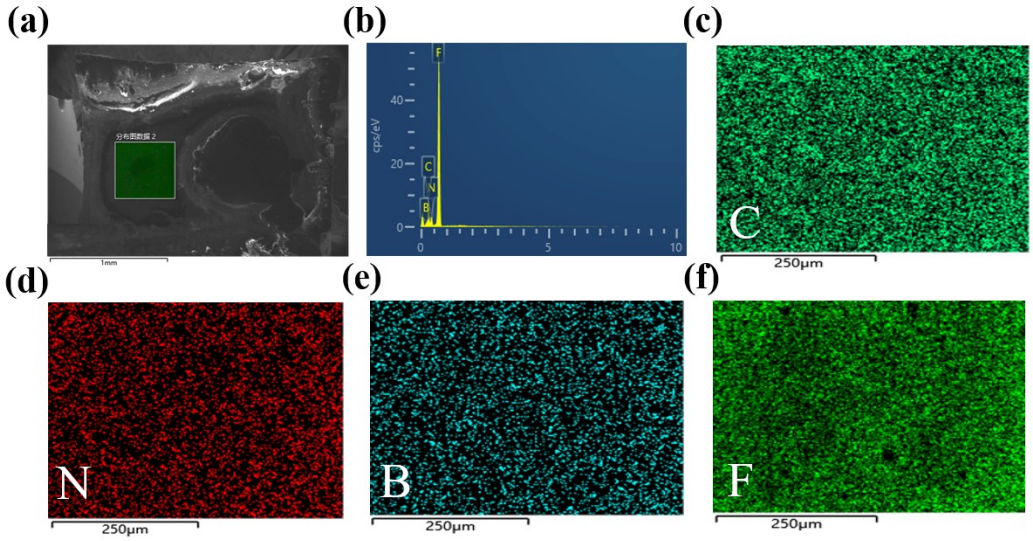


**Figure S6.** Element analysis of DABCO-$NH_4(BF_4)_3$ SC: (a) the SEM image of the EDS mapping region. (b) The corresponding EDS spectrum of DABCO-$NH_4(BF_4)_3$ and (c-f) the EDS mapping of C, N, B, and F, respectively.

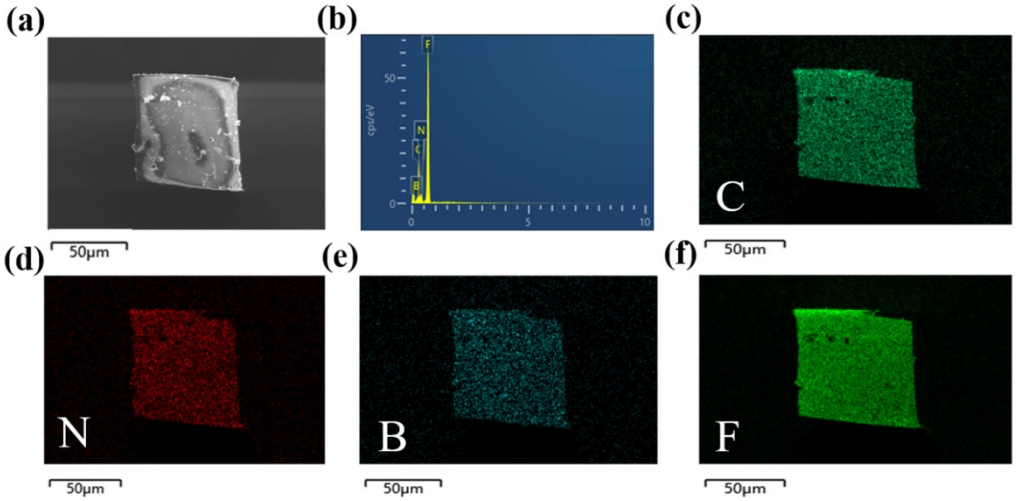


**Figure S7.** Element analysis of DABCO-$N_2H_5(BF_4)_3$ SC: (a) the SEM image of a selected microcrystal. (b) The corresponding EDS spectrum of DABCO-$N_2H_5(BF_4)_3$ and (c-f) the EDS mapping of C, N, B, and F, respectively.

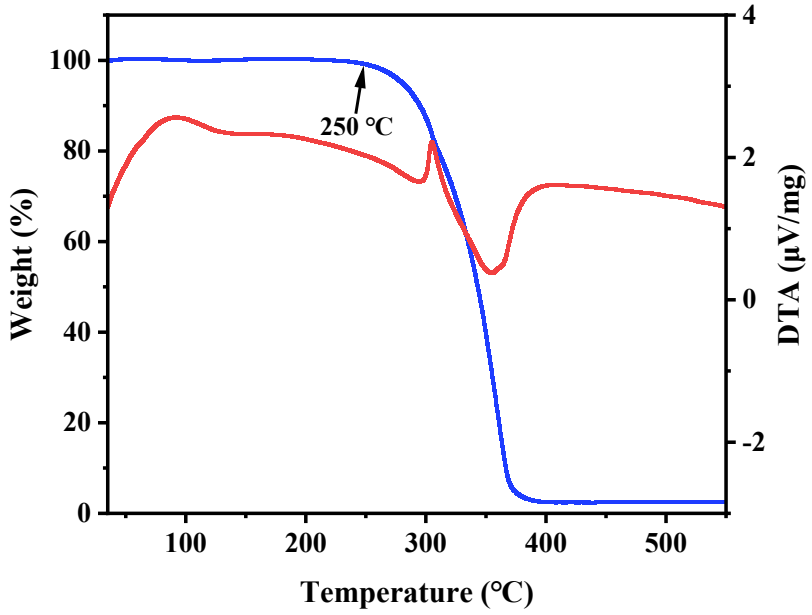


**Figure S8.** Thermogravimetric and DTA curves of DABCO-$NH_4(BF_4)_3$.

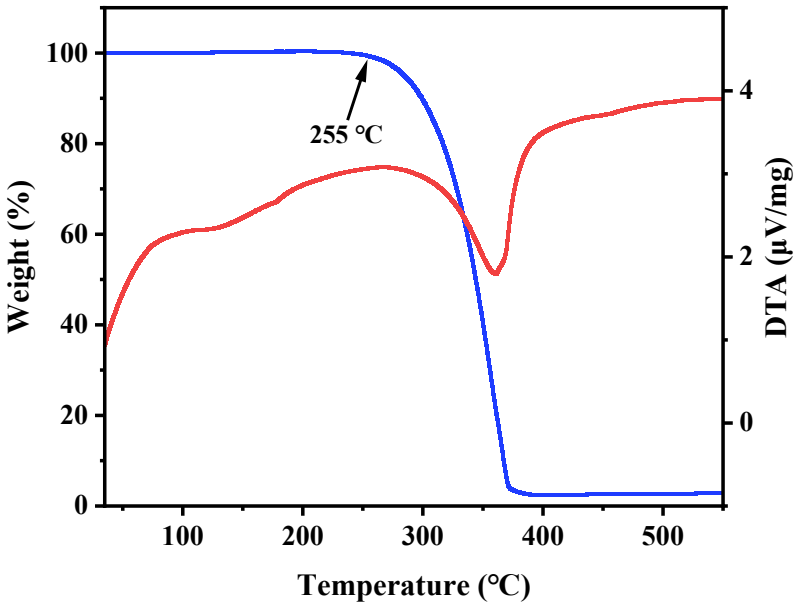


**Figure S9.** Thermogravimetric and DTA curves of DABCO-$N_2H_5(BF_4)_3$.

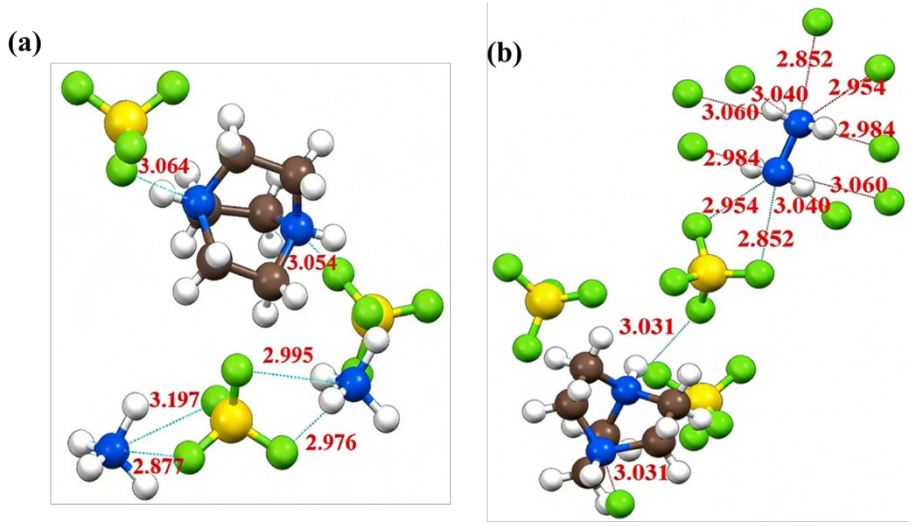


**Figure S10.** Schematic diagram of hydrogen bond lengths for (a) DABCO-$NH_4(BF_4)_3$ and (b) DABCO-$N_2H_5(BF_4)_3$. (Brown spheres are C, blue spheres are N, white spheres are H, yellow spheres are B, green spheres are F atoms).

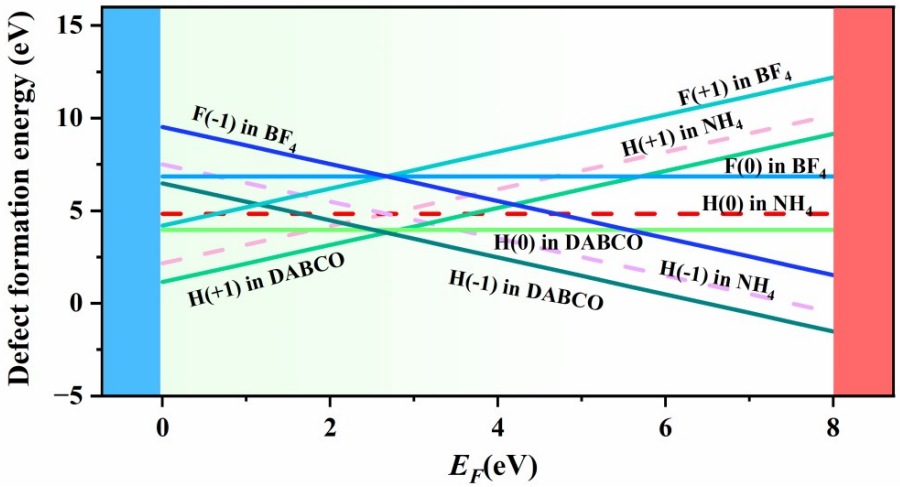


**Figure S11.** Defect formation energy of DABCO-$NH_4(BF_4)_3$.

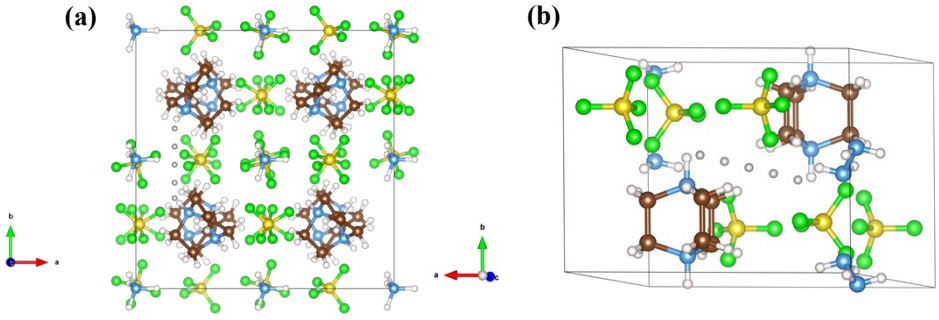


**Figure S12.** (a) The H-ion migration path of DABCO-$NH_4(BF_4)_3$; (b) The H-ion migration path of DABCO-$N_2H_5(BF_4)_3$.

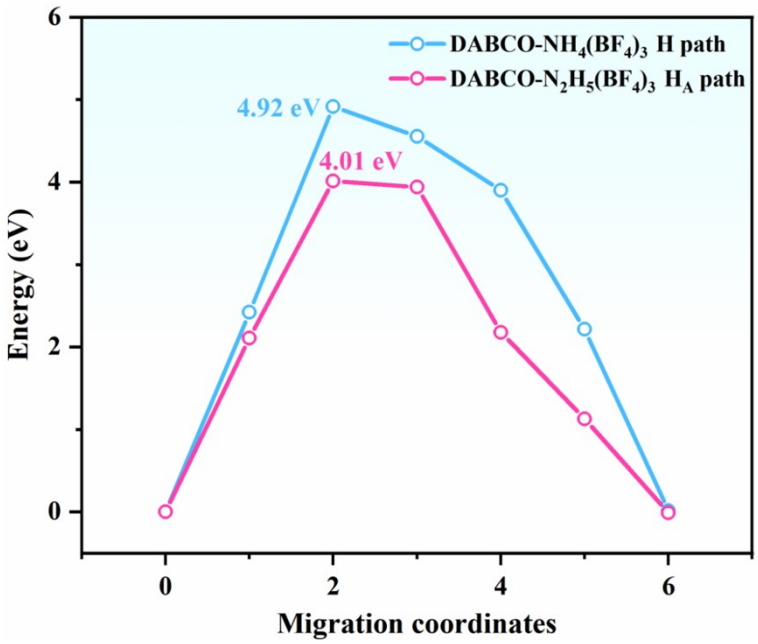


**Figure S13.** The calculated ionic migration energy of H ion in DABCO of the DABCO-$NH_4(BF_4)_3$ and $H_A$ in $N_2H_5$ of the DABCO-$N_2H_5(BF_4)_3$. $H_A$ represents the H atom attached to the N atom bearing a lone pair in the $N_2H_5$.

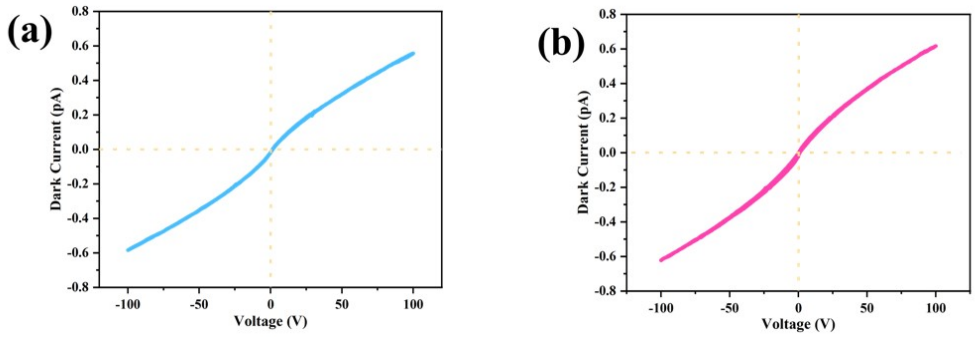


**Figure S14.** The forward and reverse I-V sweep curves of (a) DABCO-$NH_4(BF_4)_3$, (b) DABCO-$N_2H_5(BF_4)_3$

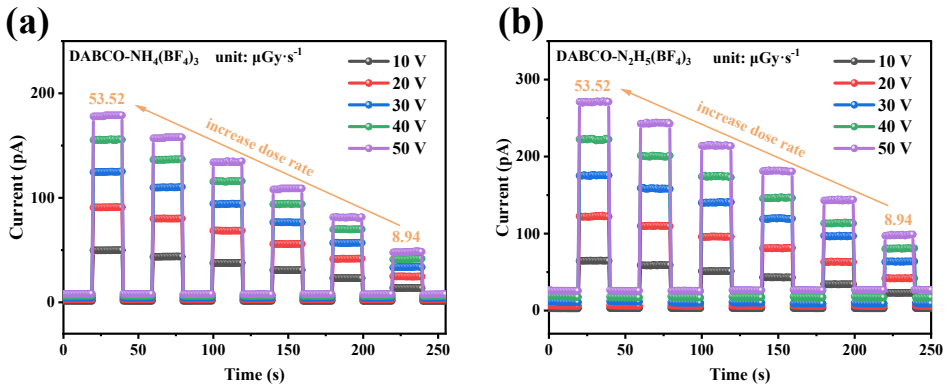


**Figure S15.** The current-time (I-T) measurements of (a) DABCO-$NH_4(BF_4)_3$ SC device and (b) DABCO-$N_2H_5(BF_4)_3$ SC device.

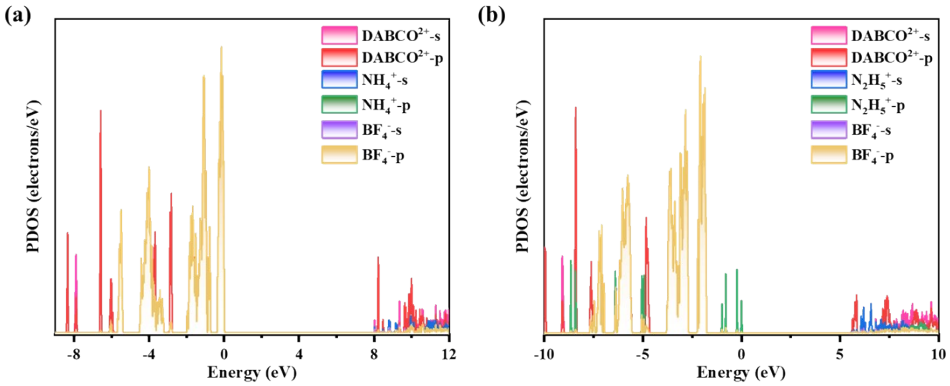


**Figure S16.** The calculated partial density of states (PDOS) of (a) DABCO-$NH_4(BF_4)_3$ and (b) DABCO-$N_2H_5(BF_4)_3$.

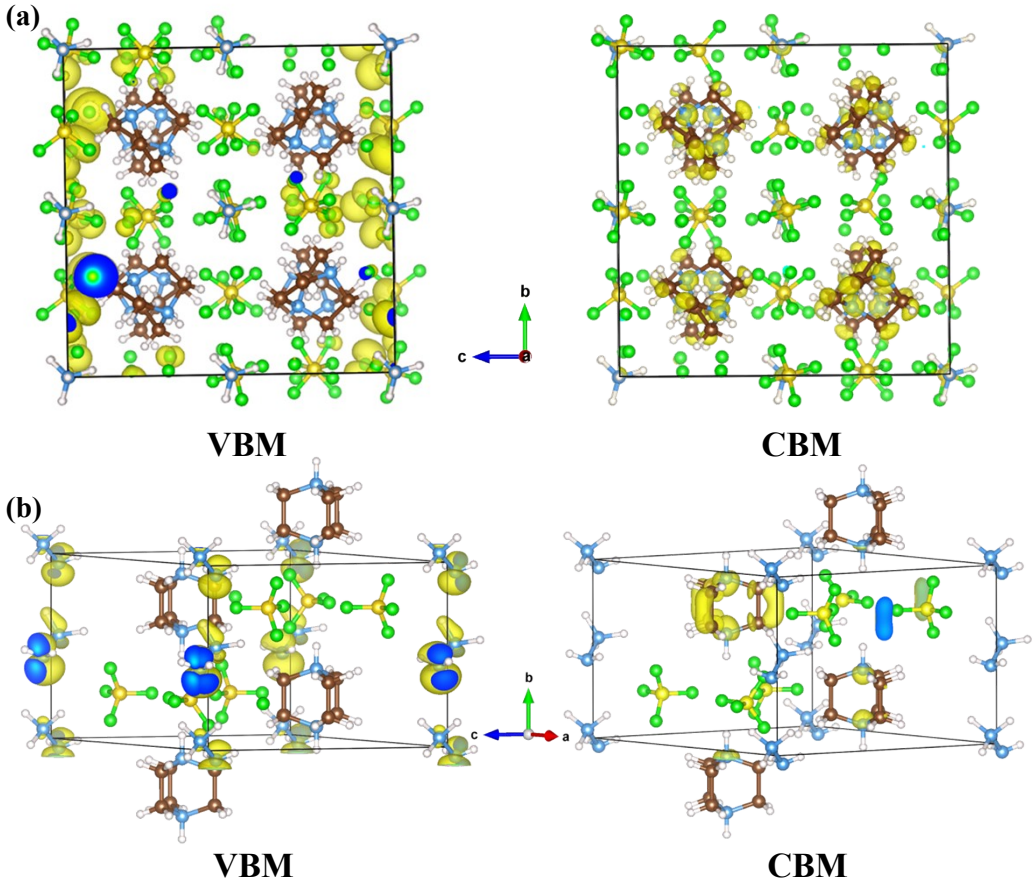


**Figure S17.** The diagrams of charge-density distributions for (a) DABCO-$NH_4(BF_4)_3$ and (b) DABCO-$N_2H_5(BF_4)_3$.

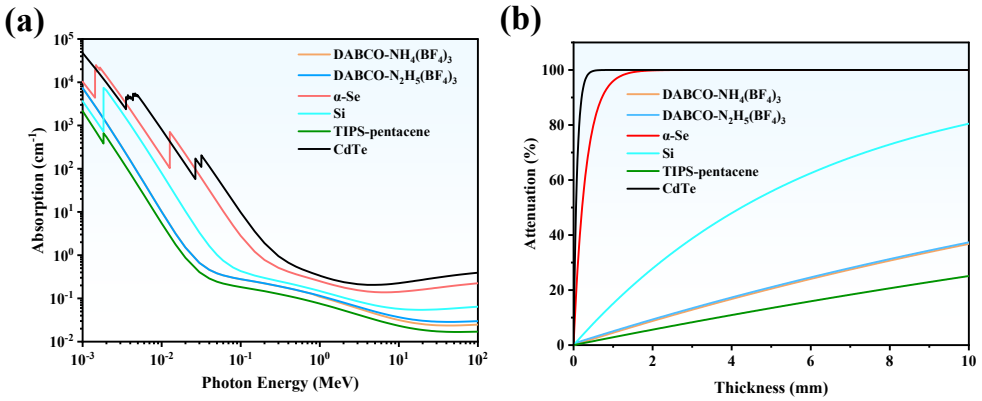


**Figure S18.** The absorption coefficient (a) and attenuation efficiency (b) of DABCO-$NH_4(BF_4)_3$, DABCO-$N_2H_5(BF_4)_3$, CdTe, TIPS-pentacene, α-Se and Si.

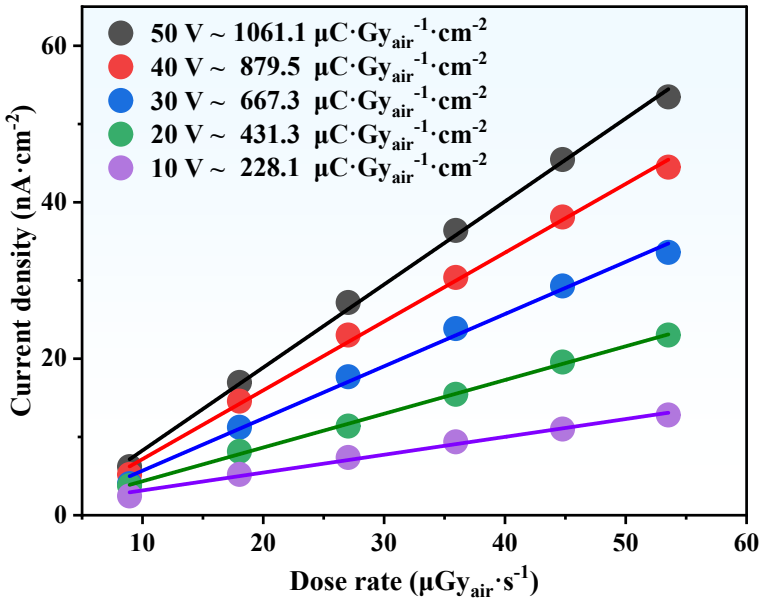


**Figure S19.** X-ray responses of current density with various dose rates for DABCO-$N_2H_5(BF_4)_3$ SC device along perpendicular direction.

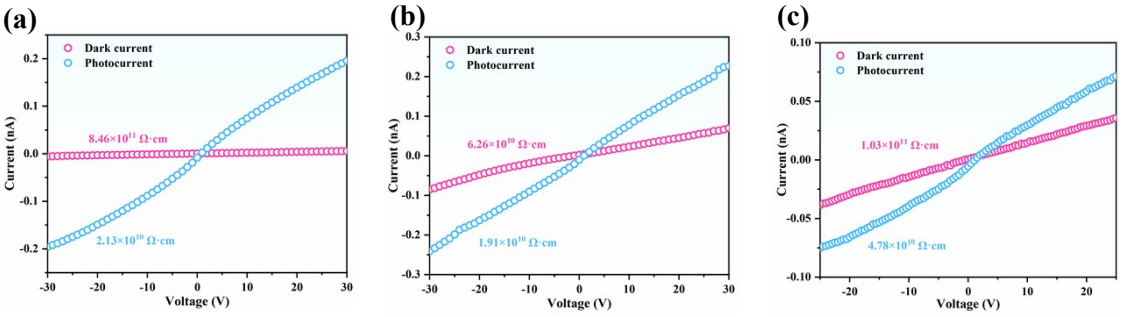


**Figure S20.** The resistivity measurement under X-ray on and off conditions of the (a) DABCO-$NH_4(BF_4)_3$ SC device and (b) DABCO-$N_2H_5(BF_4)_3$ SC device along the parallel and (c) perpendicular direction;.

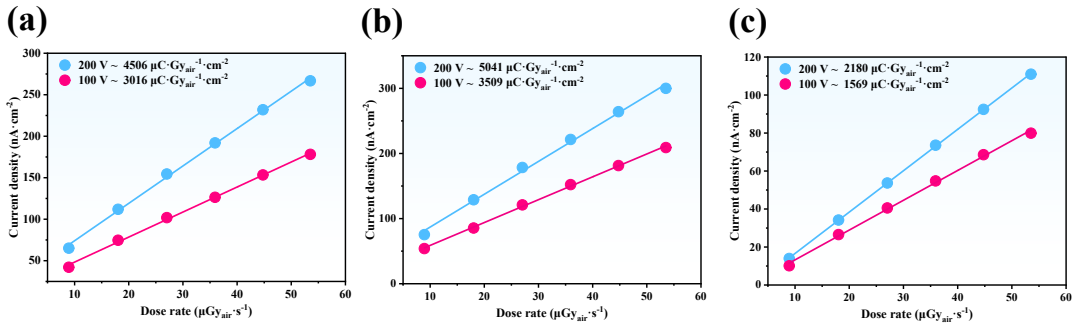


**Figure S21.** X-ray responses of current density with various dose rates at 100 V and 200 V for (a) DABCO-$NH_4(BF_4)_3$ SC device and (b) DABCO-$N_2H_5(BF_4)_3$ SC device along parallel direction and (c) DABCO-$N_2H_5(BF_4)_3$ SC device along perpendicular direction.

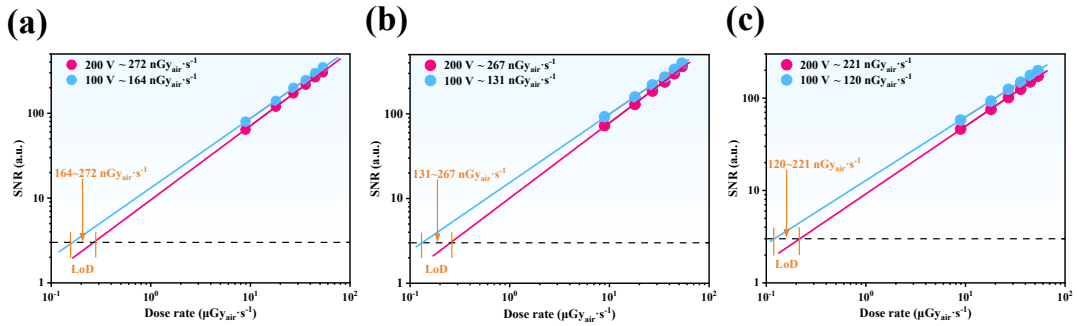


**Figure S22.** The signal-to-noise ratio for LoD calculations at 100 V and 200 V for (a) DABCO-$NH_4(BF_4)_3$ SC device and (b) DABCO-$N_2H_5(BF_4)_3$ SC device along parallel direction and (c) DABCO-$N_2H_5(BF_4)_3$ SC device along perpendicular direction.

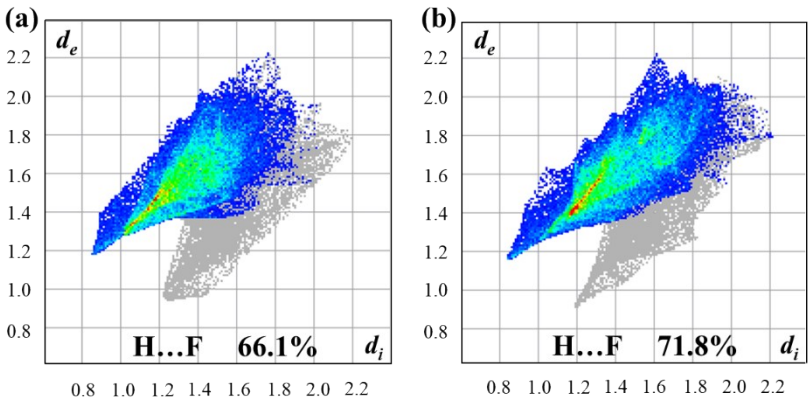


**Figure S23.** 2D fingerprints of H…F contacts in (a) DABCO-$NH_4(BF_4)_3$, (b) DABCO-$N_2H_5(BF_4)_3$.

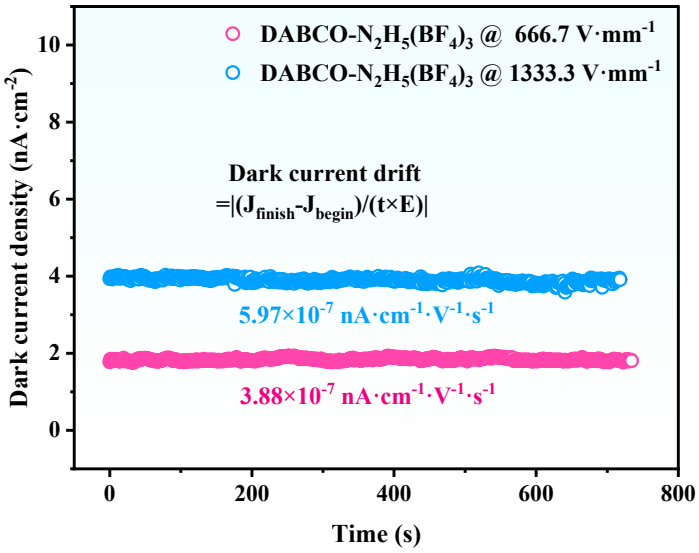


**Figure S24.** The dark current drift of DABCO-$N_2H_5(BF_4)_3$ under the electric fields of 666.6 V·mm$^{-1}$ and 1333.3 V·mm$^{-1}$.

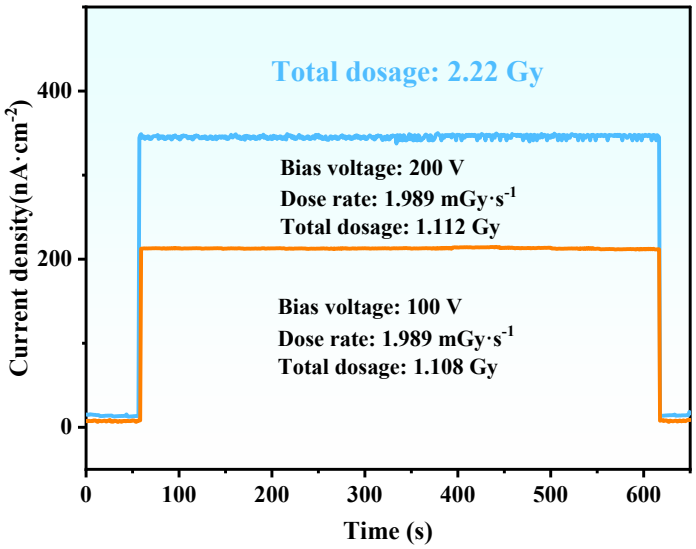


**Figure S25.** Current responses of the DABCO-$N_2H_5(BF_4)_3$ under continuous X-ray irradiation at a dose rate of 1.989 mGy·s$^{-1}$ with the bias voltages of 100 V and 200 V, respectively.

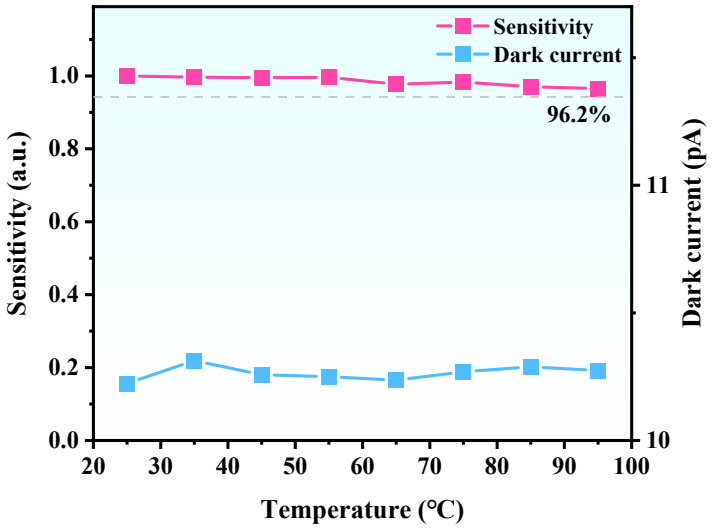


**Figure S26.** Stability of sensitivity and dark current of DABCO-$N_2H_5(BF_4)_3$ SC device under different temperatures condition.

**Table S1.** Ion radius in the DABCO-$NH_4(BF_4)_3$ and DABCO-$N_2H_5(BF_4)_3$.

| Ions | $DABCO^{2+}$ | $NH_4^+$ | $N_2H_5^+$ | $BF_4^-$ |
|---|---|---|---|---|
| Radius (pm) | 239 | 146 | 216 | 232 |

**Table S2.** Calculated Goldschmidt tolerance factors (t) of DABCO-$NH_4(BF_4)_3$ and DABCO-$N_2H_5(BF_4)_3$.

| Compound | DABCO-$NH_4(BF_4)_3$ | DABCO-$N_2H_5(BF_4)_3$ |
|---|---|---|
| *t* | 0.88 | 0.75 |

**Table S3.** Crystal data and structure refinement of DABCO-$NH_4(BF_4)_3$ and DABCO-$N_2H_5(BF_4)_3$.

| Compound | DABCO-$NH_4(BF_4)_3$ | DABCO-$N_2H_5(BF_4)_3$ |
|---|---|---|
| Empirical formula | $(C_6H_{14}N_2)$-$NH_4(BF_4)_3$ | $(C_6H_{14}N_2)$-$N_2H_5(BF_4)_3$ |
| Formula weight | 129.54 | 203.34 |
| Temperature /K | 293(2) | 293(2) |
| Crystal system | cubic | monoclinic |
| Space group | $Pa\bar{3}$ | $P2_1/m$ |
| *a* /Å | 14.2388(2) | 10.3310(8) |
| *b* /Å | 14.2388(2) | 7.9328(4) |
| *c* /Å | 14.2388(2) | 10.4916(8) |
| α /° | 90 | 90 |
| β /° | 90 | 118.426(10) |
| γ /° | 90 | 90 |
| Volume /Å$^3$ | 2886.82(12) | 756.16(11) |
| *Z* | 24 | 4 |
| $\rho_{calc}$ /gcm$^{-3}$ | 1.788 | 1.786 |
| $\mu$ /mm$^{-1}$ | 1.986 | 1.942 |
| *F*(000) | 1552 | 410 |
| Radiation | Cu$K_\alpha$ (λ=1.54184 Å) | Cu$K_\alpha$ (λ=1.54184 Å) |
| 2θ range /° | 10.76 to 158.26 (0.79 Å) | 9.59 to 152.63(0.79 Å) |
| Index ranges | $-16 \le h \le 12$<br>$-17 \le k \le 4$<br>$-13 \le l \le 17$ | $-12 \le h \le 12$<br>$-9 \le k \le 3$<br>$-12 \le l \le 13$ |
| Reflections collected | 3722 | 4400 |
| Independent reflections | 1000<br>$R_{int}$ = 0.0240<br>$R_{sigma}$ = 0.0200 | 1620<br>$R_{int}$ = 0.0318<br>$R_{sigma}$ = 0.0398 |
| Data/Restraints/Parameters | 1000/0/77 | 1620/0/133 |
| Goodness-of-fit on $F^2$ | 1.101 | 1.074 |
| Final *R* indexes [$I \ge 2\sigma(I)$] | $R_1$ = 0.0479<br>w$R_2$ = 0.1432 | $R_1$ = 0.0547<br>w$R_2$ = 0.1561 |
| Final *R* indexes [all data] | $R_1$ = 0.0519<br>w$R_2$ = 0.1474 | $R_1$ = 0.0650<br>w$R_2$ = 0.1638 |
| Largest peak/hole/ eÅ$^{-3}$ | 0.58/−0.21 | 0.28/−0.22 |

**Table S4.** Bond lengths (Å) and angles (°)for DABCO-$NH_4(BF_4)_3$

| Label | Distances (Å) | Label | Angles (°) |
|---|---|---|---|
| F1–B2 | 1.400(3) | C10–N8–C10#1 | 109.58(13) |
| F3–B2 | 1.391(3) | C10–N8–C10#2 | 109.58(13) |
| F4–B2 | 1.383(3) | C10#1–N8–C10#2 | 109.58(13) |
| F5–B2 | 1.384(3) | C10–N8–H8 | 109.4 |
| N8–C10 | 1.494(2) | C10#1–N8–H8 | 109.4 |
| N8–C10#1 | 1.494(2) | C10#2–N8–H8 | 109.4 |
| N8–C10#2 | 1.494(2) | C11#1–N9–C11#2 | 109.57(14) |
| N8–H8 | 0.9800 | C11#1–N9–C11 | 109.57(14) |
| N9–C11#1 | 1.493(2) | C11#2–N9–C11 | 109.57(14) |
| N9–C11#2 | 1.493(2) | C11#1–N9–H9 | 109.37(14) |
| N9–C11 | 1.493(2) | C11#2–N9–H9 | 109.37(14) |
| N9–H9 | 1.01(5) | C11–N9–H9 | 109.37(14) |
| C10–C11 | 1.523(3) | N8–C10–C11 | 108.15(19) |
| C10–H10A | 0.9700 | N8–C10–H10A | 110.1 |
| C10–H10B | 0.9700 | C11–C10–H10A | 110.1 |
| C11–H11A | 0.9700 | N8–C10–H10B | 110.1 |
| C11–H11B | 0.9700 | C11–C10–H10B | 110.1 |
| | | H10A–C10–H10B | 108.4 |
| | | N9–C11–C10 | 108.19(19) |
| | | N9–C11–H11A | 110.1 |
| | | C10–C11–H11A | 110.1 |
| | | N9–C11–H11B | 110.1 |
| | | C10–C11–H11B | 110.1 |
| | | H11A–C11–H11B | 108.4 |
| | | F4–B2–F5 | 110.2(2) |
| | | F4–B2–F3 | 110.32(18) |
| | | F5–B2–F3 | 108.97(19) |
| | | F4–B2–F1 | 109.50(18) |
| | | F5–B2–F1 | 109.42(17) |
| | | F3–B2–F1 | 108.44(19) |

Symmetry transformations used to generate equivalent atoms:

#1: 1.5-z, 1-x, 0.5+y; #2: 1-y, -0.5+z, 1.5 -x.

**Table S5.** Bond lengths (Å) and angles (°) for DABCO-$N_2H_5(BF_4)_3$

| Label | Distances (Å) | Label | Angles (°) |
|---|---|---|---|
| F2–B1 | 1.382(5) | C14–N13–C16 | 109.4(2) |
| F3–B1 | 1.379(3) | C14–N13–C15 | 110.4(2) |
| F4–B1 | 1.384(5) | C16–N13–C15 | 109.9(2) |
| F5–B6 | 1.376(3) | C14–N13–H13 | 109.0 |
| F8–B6 | 1.377(5) | C16–N13–H13 | 109.0 |
| F7–B6 | 1.377(5) | C15–N13–H13 | 109.0 |
| F10–B9 | 1.391(6) | N1#1–N1–H1A | 101(3) |
| F11–B9 | 1.365(4) | N1#1–N1–H1B | 104(3) |
| N13–C14 | 1.485(4) | H1A–N1–H1B | 110(4) |
| N13–C16 | 1.491(4) | N13–C15–C15#2 | 108.83(14) |
| N13–C15 | 1.492(3) | N13–C15–H15A | 109.9 |
| N13–H13 | 0.9800 | C15#2–C15–H15A | 109.9 |
| F12–B9 | 1.369(5) | N13–C15–H15B | 109.9 |
| N1–N1#1 | 1.424(5) | C15#2–C15–H15B | 109.9 |
| N1–H1A | 0.86(4) | H15A–C15–H15B | 108.3 |
| N1–H1B | 0.84(4) | N13–C16–C16#2 | 109.23(15) |
| C15–C15#2 | 1.520(6) | N13–C16–H16A | 109.8 |
| C15–H15A | 0.9700 | C16#2–C16–H16A | 109.8 |
| C15–H15B | 0.9700 | N13–C16–H16B | 109.8 |
| C16–C16#2 | 1.501(7) | C16#2–C16–H16B | 109.8 |
| C16–H16A | 0.9700 | H16A–C16–H16B | 108.3 |
| C16–H16B | 0.9700 | N13–C14–C14#2 | 109.06(15) |
| C14–C14#2 | 1.514(7) | N13–C14–H14A | 109.9 |
| C14–H14A | 0.9700 | C14#2–C14–H14A | 109.9 |
| C14–H14B | 0.9700 | N13–C14–H14B | 109.9 |
| | | C14#2–C14–H14B | 109.9 |
| | | H14A–C14–H14B | 108.3 |
| | | F5#3–B6–F5 | 109.7(3) |
| | | F5#3–B6–F7 | 109.3(2) |
| | | F5–B6–F7 | 109.3(2) |
| | | F5#3–B6–F8 | 109.4(2) |
| | | F5–B6–F8 | 109.4(2) |
| | | F7–B6–F8 | 109.6(4) |
| | | F3–B1–F3#3 | 108.9(3) |
| | | F3–B1–F2 | 109.3(2) |
| | | F3#3–B1–F2 | 109.3(2) |
| | | F3–B1–F4 | 109.8(2) |
| | | F3#3–B1–F4 | 109.8(2) |

Symmetry transformations used to generate equivalent atoms: #1: -x, -y, -z; #2: +x, 1.5-y, +z; #3: +x, 0.5-y, +z**.**

**Table S6.** Atomic coordinates (× $10^4$) and equivalent isotropic displacement parameters (Å$^2$ × $10^3$) for DABCO-$NH_4(BF_4)_3$

| Atom | *x* | *y* | *z* | $U_{eq}$ |
|---|---|---|---|---|
| F1 | 0.51496(10) | 0.30700(10) | 0.92336(9) | 0.0430(4) |
| F3 | 0.55770(10) | 0.18744(10) | 1.01906(11) | 0.0495(5) |
| F4 | 0.40492(10) | 0.20345(10) | 0.97471(12) | 0.0516(5) |
| F5 | 0.47055(13) | 0.30685(11) | 1.07663(10) | 0.0553(5) |
| N6 | 0.500000 | 0.000000 | 1.000000 | 0.0299(9) |
| N7 | 0.500000 | 0.500000 | 1.000000 | 0.0298(9) |
| N8 | 0.79409(12) | 0.20591(12) | 0.70591(12) | 0.0293(7) |
| H8 | 0.833825 | 0.166174 | 0.666173 | 0.035 |
| N9 | 0.69307(11) | 0.30693(11) | 0.80693(11) | 0.0285(6) |
| C10 | 0.70761(16) | 0.23267(17) | 0.65291(15) | 0.0387(6) |
| H10A | 0.679150 | 0.177349 | 0.625154 | 0.046 |
| H10B | 0.723366 | 0.276153 | 0.602892 | 0.046 |
| C11 | 0.63944(17) | 0.2786(2) | 0.72137(18) | 0.0469(7) |
| H11A | 0.610737 | 0.333284 | 0.692618 | 0.056 |
| H11B | 0.590098 | 0.234744 | 0.738181 | 0.056 |
| B2 | 0.48621(17) | 0.25084(15) | 0.99874(16) | 0.0306(5) |
| H9 | 0.6520(19) | 0.3480(19) | 0.8480(19) | 0.045(12) |

U(eq) is defined as one third of the trace of the orthogonalized $U_{ij}$ tensor.

**Table S7.** Atomic coordinates (× $10^4$) and equivalent isotropic displacement parameters (Å$^2$ × $10^3$) for DABCO-$N_2H_5(BF_4)_3$.

| Atom | *x* | *y* | *z* | $U_{eq}$ |
|---|---|---|---|---|
| F2 | 0.2607(3) | 0.250000 | 0.2887(3) | 0.0538(6) |
| F3 | 0.1237(2) | 0.1086(2) | 0.3679(2) | 0.0600(5) |
| F4 | 0.3263(3) | 0.250000 | 0.5277(3) | 0.0657(8) |
| F5 | 0.6552(2) | 0.1083(2) | 0.7711(2) | 0.0696(6) |
| F8 | 0.5132(3) | 0.250000 | 0.8434(3) | 0.0681(8) |
| F7 | 0.7595(3) | 0.250000 | 0.9817(3) | 0.0721(9) |
| F10 | 0.0041(3) | 0.250000 | 0.7730(4) | 0.0714(8) |
| F11 | 0.2154(3) | 0.3912(3) | 0.8933(3) | 0.0835(7) |
| N13 | 0.3334(2) | 0.5935(3) | 0.6712(2) | 0.0399(5) |
| H13 | 0.333036 | 0.469933 | 0.671349 | 0.048 |
| F12 | 0.1720(4) | 0.250000 | 0.6922(4) | 0.0930(12) |
| N1 | 0.0410(3) | 0.0545(3) | 0.0599(3) | 0.0472(6) |
| H1A | 0.130(5) | 0.028(6) | 0.080(4) | 0.071 |
| H1B | 0.023(4) | 0.017(6) | 0.125(4) | 0.071 |
| C15 | 0.3883(3) | 0.6542(4) | 0.5711(3) | 0.0467(7) |
| H15A | 0.325354 | 0.612540 | 0.473872 | 0.056 |
| H15B | 0.487268 | 0.612538 | 0.602774 | 0.056 |
| C16 | 0.1804(3) | 0.6554(4) | 0.6211(4) | 0.0539(8) |
| H16A | 0.143964 | 0.613891 | 0.685015 | 0.065 |
| H16B | 0.116217 | 0.613891 | 0.524100 | 0.065 |
| C14 | 0.4301(4) | 0.6546(4) | 0.8209(3) | 0.0544(8) |
| H14A | 0.529482 | 0.613038 | 0.854934 | 0.065 |
| H14B | 0.394563 | 0.613045 | 0.885555 | 0.065 |
| B6 | 0.6457(5) | 0.250000 | 0.8418(5) | 0.0381(9) |
| B1 | 0.2091(4) | 0.250000 | 0.3884(5) | 0.0365(8) |
| B9 | 0.1532(5) | 0.250000 | 0.8129(5) | 0.0426(10) |

U(eq) is defined as one third of the trace of the orthogonalized $U_{ij}$ tensor.

**Table S8.** Anisotropic displacement parameters ($Å^2 \times 10^3$) for DABCO-$NH_4(BF_4)_3$.

The anisotropic displacement factor exponent takes the form: $-2\pi^2$ [ $h^2$ a*$^2$ U11 + ... + 2hka* b*U12 ]

| Atom | $U_{11}$ | $U_{22}$ | $U_{33}$ | $U_{23}$ | $U_{13}$ | $U_{12}$ |
|---|---|---|---|---|---|---|
| F1 | 0.0481(8) | 0.0417(8) | 0.0392(7) | 0.0079(5) | 0.0030(6) | −0.0019(6) |
| F3 | 0.0470(9) | 0.0448(8) | 0.0568(9) | 0.0088(6) | −0.0051(7) | 0.0098(6) |
| F4 | 0.0413(8) | 0.0524(9) | 0.0610(10) | −0.0007(7) | −0.0052(7) | −0.0138(6) |
| F5 | 0.0765(12) | 0.0499(9) | 0.0396(8) | −0.0118(6) | 0.0080(7) | −0.0005(7) |
| N6 | 0.0299(9) | 0.0299(9) | 0.0299(9) | −0.0035(10) | 0.0035(10) | −0.0035(10) |
| N7 | 0.0298(9) | 0.0298(9) | 0.0298(9) | −0.0013(9) | 0.0013(9) | 0.0013(9) |
| N8 | 0.0293(7) | 0.0293(7) | 0.0293(7) | −0.0033(6) | 0.0033(6) | 0.0033(6) |
| N9 | 0.0285(6) | 0.0285(6) | 0.0285(6) | −0.0035(6) | 0.0035(6) | 0.0035(6) |
| C10 | 0.0424(12) | 0.0426(12) | 0.0310(11) | −0.0089(9) | −0.0093(9) | 0.0064(9) |
| C11 | 0.0370(12) | 0.0550(14) | 0.0488(14) | −0.0157(11) | −0.0151(10) | 0.0153(10) |
| B2 | 0.0326(11) | 0.0295(11) | 0.0298(11) | −0.0007(8) | 0.0001(9) | −0.0007(9) |

**Table S9.** Anisotropic displacement parameters ($Å^2 \times 10^3$) for DABCO-$N_2H_5(BF_4)_3$.

The anisotropic displacement factor exponent takes the form: $-2\pi^2$ [ $h^2$ a*$^2$ U11 + ... + 2hka* b*U12 ]

| Atom | $U_{11}$ | $U_{22}$ | $U_{33}$ | $U_{23}$ | $U_{13}$ | $U_{12}$ |
|---|---|---|---|---|---|---|
| F2 | 0.0480(13) | 0.0667(16) | 0.0527(14) | 0.000 | 0.0289(11) | 0.000 |
| F3 | 0.0695(12) | 0.0449(10) | 0.0655(11) | 0.0000(8) | 0.0322(10) | −0.0164(8) |
| F4 | 0.0549(15) | 0.083(2) | 0.0400(13) | 0.000 | 0.0069(11) | 0.000 |
| F5 | 0.0857(14) | 0.0450(11) | 0.0835(14) | −0.0171(9) | 0.0446(12) | 0.0012(9) |
| F8 | 0.0477(14) | 0.099(2) | 0.0647(17) | 0.000 | 0.0321(13) | 0.000 |
| F7 | 0.0544(16) | 0.089(2) | 0.0519(15) | 0.000 | 0.0085(12) | 0.000 |
| F10 | 0.0597(16) | 0.077(2) | 0.080(2) | 0.000 | 0.0361(15) | 0.000 |
| F11 | 0.1006(17) | 0.0564(13) | 0.0986(17) | −0.0256(12) | 0.0515(14) | −0.0276(12) |
| N13 | 0.0534(13) | 0.0255(10) | 0.0449(12) | −0.0016(9) | 0.0268(11) | −0.0004(9) |
| F12 | 0.104(3) | 0.133(3) | 0.0648(19) | 0.000 | 0.0589(19) | 0.000 |
| N1 | 0.0462(13) | 0.0555(15) | 0.0353(11) | −0.0063(11) | 0.0156(10) | −0.0004(11) |
| C15 | 0.0569(16) | 0.0452(16) | 0.0510(15) | −0.0057(13) | 0.0363(13) | −0.0001(13) |
| C16 | 0.0409(14) | 0.0562(18) | 0.071(2) | −0.0135(16) | 0.0315(14) | −0.0108(14) |
| C14 | 0.0706(19) | 0.0457(17) | 0.0368(14) | 0.0071(12) | 0.0173(13) | 0.0133(15) |
| B6 | 0.039(2) | 0.032(2) | 0.043(2) | 0.000 | 0.0197(18) | 0.000 |
| B1 | 0.036(2) | 0.035(2) | 0.037(2) | 0.000 | 0.0169(17) | 0.000 |
| B9 | 0.055(3) | 0.031(2) | 0.050(2) | 0.000 | 0.032(2) | 0.000 |

**Table S10.** Band gaps and resistivity of different MFPs

| Compound | Band gap | Resistivity (Ω·cm) | Ref |
|---|---|---|---|
| DABCO-$NH_4(BF_4)_3$ | 8.13 eV | $8.46\times10^{11}$ | This work |
| DABCO-$N_2H_5(BF_4)_3$ (∥) | 5.48 eV | $6.26\times10^{10}$ | This work |
| DABCO-$N_2H_5(BF_4)_3$ (⊥) | 5.48 eV | $1.03\times10^{11}$ | This work |
| DABCO-$N_2H_5Br_3$ | 5.47 eV | $2.74\pm1.42\times10^{10}$ | [12] |
| DABCO-$N_2H_5I_3$ | 4.79 eV | $1.26\pm0.02\times10^{10}$ | [12] |
| MDABCO-$NH_4I_3$ | 4.95 eV | $1.90\times10^{7}$ | [13] |
| MDABCO-$NH_4(PF_6)_3$ | 7.96 eV | $7.94\times10^{9}$ | [14] |
| NDABCO-$NH_4Br_3$ | 3.14 eV | $1.67\times10^{9}$ | [15] |
| (3-AP)-$NH_4I_3$ | 4.50 eV | $3.63\times10^{9}$ | [16] |

**Table S11.** Summary on the key parameters of MFPs X-ray detectors.

| Compound | Electric field / bias | Type | Sensitivity ($\mu C \cdot Gy_{air}^{-1} \cdot cm^{-2}$) | LoD ($nGy_{air} \cdot s^{-1}$) | Ref |
|---|---|---|---|---|---|
| DABCO-$N_2H_5Br_3$ | 200 V | SC | 1143 | 2680 | [12] |
| DABCO-$N_2H_5I_3$ | 200 V | SC | 1187 | 2880 | [12] |
| MDABCO-$NH_4I_3$ | 50 V | SC | 1997 | ＞5500 | [13] |
| MDABCO-$NH_4(PF_6)_3$ | 50 V | SC | 2078 | 16.3 | [14] |
| NDABCO-$NH_4Br_3$ | 10 V | SC | 623 | 970 | [15] |
| (3-AP)-$NH_4I_3$ | 50 V | SC | 1556 | 1140 | [16] |
| DABCO-$NH_4Cl_3$ | 50 V | SC | 165 | ＞5500 | [17] |
| DABCO-$NH_4Br_3$ | 50 V | SC | 176 | 4960 | [17] |
| DABCO-$NH_4I_3$ | 50 V | SC | 567 | ＞5500 | [17] |
| MDABCO-$NH_4(BF_4)_3$ | 200 $V \cdot mm^{-1}$ | SC | 617 | 155 | [18] |
| MDABCOCl-$NH_4(BF_4)_3$ | 200 $V \cdot mm^{-1}$ | SC | 1522 | 68.2 | [18] |
| MDABCOBr-$NH_4(BF_4)_3$ | 200 $V \cdot mm^{-1}$ | SC | 2337 | 50.1 | [18] |
| DABCO-$NH_4(BF_4)_3$ | 50 V | SC | 1931 | 30.2 | This work |
| DABCO-$N_2H_5(BF_4)_3$ | 50 V | SC | 2570 (∥)<br>1061 (⊥) | 20.9 (∥)<br>35.3 (⊥) | This work |

**Table S12.** Ion migration energy of DABCO-$NH_4(BF_4)_3$ and DABCO-$N_2H_5(BF_4)_3$ in comparison with most reported MFPs and lead-based perovskites.

| Material | Ion migration energy | Ref |
|---|---|---|
| DABCO-$NH_4(BF_4)_3$ | 4.01 | This Work |
| DABCO-$N_2H_5(BF_4)_3$ | 4.92 | This Work |
| (DABCO)-$N_2H_5(NH_4)_2Cl_9$ | 0.75 | [12] |
| DABCO-$N_2H_5Br_3$ | 0.99 | [12] |
| DABCO-$N_2H_5I_3$ | 1.09 | [12] |
| MDABCO-$NH_4I_3$ | ~0.80 | [13] |
| MDABCO-$NH_4(BF_4)_3$ | ~4.10 | [18] |
| (MDABCOCl)-$NH_4(BF_4)_3$ | ~4.25 | [18] |
| (MDABCOBr)-$NH_4(BF_4)_3$ | ~5.10 | [18] |
| MDABCO-$NH_4(PF_6)_3$ | ~6.00 | [14] |
| $(CHMA)_2PbCl_4$ | 0.69 | [19] |
| (4-AMPD)$PbCl_4$ | 1.00 | [19] |
| $(PbCl_2)_2$(4-AMTP)$_2PbCl_4$ | 1.64 | [19] |

## References


1 O. V. Dolomanov, L. J. Bourhis, R. J. Gildea, J. A. K. Howard and H. Puschmann, *J Appl Crystallogr*, 2009, **42**, 339–341.

2 A. L. Spek, *J Appl Crystallogr*, 2003, **36**, 7–13.

3 S. J. Clark, M. D. Segall, C. J. Pickard, P. J. Hasnip, M. I. J. Probert, K. Refson and M. C. Payne, *Zeitschrift für Kristallographie - Crystalline Materials*, 2005, **220**, 567–570.

4 M. C. Payne, M. P. Teter, D. C. Allan, T. A. Arias and J. D. Joannopoulos, *Rev. Mod. Phys.*, 1992, **64**, 1045–1097.

5 H. J. Monkhorst and J. D. Pack, *Phys. Rev. B*, 1976, **13**, 5188–5192.

6 J. VandeVondele, M. Krack, F. Mohamed, M. Parrinello, T. Chassaing and J. Hutter, *Computer Physics Communications*, 2005, **167**, 103–128.

7 G. Henkelman, B. P. Uberuaga and H. Jónsson, *The Journal of Chemical Physics*, 2000, **113**, 9901–9904.

8 C. Freysoldt, B. Grabowski, T. Hickel, J. Neugebauer, G. Kresse, A. Janotti and C. G. Van De Walle, *Rev. Mod. Phys.*, 2014, **86**, 253–305.

9 T. Lu and Q. Chen, *J Comput Chem*, 2022, **43**, 539–555.

10 T. Lu and F. Chen, *J Comput Chem*, 2012, **33**, 580–592.

11 W. Humphrey, A. Dalke and K. Schulten, *Journal of Molecular Graphics*, 1996, **14**, 33–38.

12 X. Song, H. Cohen, J. Yin, H. Li, J. Wang, Y. Yuan, R. Huang, Q. Cui, C. Ma, S. (Frank) Liu, G. Hodes and K. Zhao, *Small*, 2023, **19**, 2300892.

13 X. Song, Q. Li, J. Han, C. Ma, Z. Xu, H. Li, P. Wang, Z. Yang, Q. Cui, L. Gao, Z. Quan, S. (Frank) Liu and K. Zhao, *Advanced Materials*, 2021, **33**, 2102190.

14 Z. Z. Li, Z. H. Li, G. Q. Peng, C. Shi, H. X. Wang, S. Ding, Q. Wang, Z. T. Liu and Z. W. Jin, *Advanced Materials*, 2023, **35**, 2300480.

15 Z. Li, Y. Pang, G. Peng, H. Wang, Q. Li, X. Zhou, Z. Li, Q. Wang and Z. Jin, *J. Phys. Chem. Lett.*, 2024, **15**, 4375–4383.

16 Q. Y. Cui, X. M. Liu, N. Li, H. Q. Zeng, D. P. Chu, H. J. Li, X. Song, Z. Xu, Y. P. Liu, H. M. Zhu, K. Zhao and S. Liu, *Small*, 2024, **20**, 2308945.

17 Q. Cui, X. Song, Y. Liu, Z. Xu, H. Ye, Z. Yang, K. Zhao and S. (Frank) Liu, *Matter*, 2021, **4**, 2490–2507.

18 Y. Lei, M. Yin, C. Shi, L. Wu, G. Peng, Y. Xu, H. Wang, R. Tang, Z. Li and Z. Jin, *npj Flexible Electron.*, 2024, **8**, 46–55.

19 Y. Ma, W. Li, Y. Liu, W. Guo, H. Xu, L. Tang, Q. Fan, L. Wei, J. Luo and Z. Sun, *Adv. Sci.*, 2025, **12**, e07588.